Electronic Supplementary Material (ESI) for Green Chemistry.

Supporting information

Conversion of lipid into high-viscosity branched bio-lubricant base oil

Shuang Chen, Tingting Wu, Chen Zhao*

Shanghai Key Laboratory of Green Chemistry and Chemical Processes, School of Chemistry and Molecular Engineering, East China Normal University, Shanghai 200062, China

Email: czhao@chem.ecnu.edu.cn

Experimental section:

Chemicals:

Stearic acid ($C_{18}H_{36}O_2$, Sinopharm Chemical Reagent Co., Ltd.), methyl stearate ($C_{19}H_{38}O_2$, Sinopharm Chemical Reagent Co., Ltd.), coconut oil (COFCO Fulinmen Food Marketing Co., Ltd.), palm oil (COFCO Fulinmen Food Marketing Co., Ltd.) Co., Ltd.), seaweed oil (COFCO Fulinmen Food Marketing Co., Ltd.), soybean oil (COFCO Fulinmen Food Marketing Co., Ltd.), *n*-dodecanol ($C_{12}H_{26}O$, Sinopharm Chemical Reagent Co., Ltd.), *n*-tetradecanol ($C_{14}H_{30}O$, Sinopharm Chemical Reagent Co., Ltd.), n-hexadecanol ($C_{16}H_{34}O$, Sinopharm Chemical Reagent Co., Ltd.), *n*-octadecanol ($C_{18}H_{38}O$, Sinopharm Chemical Reagent Co., Ltd.), α-octene (C_8H_{16}, Shanghai Aladdin Biochemical Technology Co., Ltd.), α-decene ($C_{10}H_{20}$, Shanghai Aladdin Biochemical Technology Co., Ltd.), α-tetradecene ($C_{14}H_{28}$, Shanghai Aladdin Biochemical Technology Co., Ltd.), α-hexadecene ($C_{16}H_{32}$, Shanghai Aladdin Latin Biochemical Technology Co., Ltd.), α-octadecene ($C_{18}H_{36}$, Shanghai Aladdin Biochemical Technology Co., Ltd.), silicon dioxide (SiO_2, Shanghai Maikun Chemical Co., Ltd.), aluminum oxide (Al_2O_3, Shanghai Maikun Chemical Co., Ltd.), tin chloride ($SnCl_4{\cdot}5H_2O$, Sinopharm Chemical Reagent Co., Ltd.), cobalt nitrate ($Co\ (NO_3)_2{\cdot}6H_2O$, Sinopharm Chemical Reagent Co., Ltd.), thorium nitrate ($Th\ (NO_3)_4{\cdot}6H_2O$, $Th(NO_3)_4{\cdot}6H_2O$), copper nitrate ($Cu(NO_3)_2{\cdot}6H_2O$, $Cu(NO_3)_2{\cdot}6H_2O$), ammonium perrhenate (NH_4ReO_4, Sinopharm Chemical Reagent Co., Ltd.), ruthenium chloride ($RuCl_3{\cdot}3H_2O$, Sinopharm Chemical Reagent Co., Ltd.), palladium nitrate ($Pd\ (NO_3)_2$, Sinopharm Chemical Reagent Co., Ltd.), tungsten oxide (WO_3, Sinopharm Chemical Reagent Co., Ltd.), niobium oxide (Nb_2O_5, Sinopharm Chemical Reagent Co., Ltd.), molybdenum oxide (MoO_2, Sinopharm Chemical Reagent Co., Ltd.), zirconia (ZrO_2, Sinopharm Chemical Reagent Co., Ltd.), zirconyl sulfate ($ZrOSO_4$, Sinopharm Chemical Reagent Co., Ltd.), sulfonated carbon (Sinopharm Chemical Reagent Co., Ltd.), ion exchange resin (Sinopharm Chemical Reagent Co., Ltd.), *n*-hexane (Sinopharm Chemical Reagent Co., Ltd.), Air (Shanghai Pujiang Specialty Gas Co., Ltd.), Hydrogen (Shanghai Pujiang Specialty Gas Co., Ltd.), Nitrogen (N_2, Shanghai Pujiang Specialty Gas Co., Ltd.).

Catalyst preparation

Hydrogenation catalyst: Weigh a certain amount of metal salt precursor such as $RuCl_3$ and dissolve it in distilled water. After it is completely dissolved, add a certain amount of support SiO_2, continue to stir at room temperature for 1.0 h, then raise the temperature to 50 ˚C. Until the solution was completely spin-dried, and the solid powder was further dried in an oven at 100 ˚C for 12 h, and calcined at 450 ˚C in an air atmosphere for 4.0 h (air flow rate: 100 $mL\cdot min^{-1}$, heating rate: 2.0 $^{\circ}C\cdot min^{-1}$). Reduction was conducted in a hydrogen atmosphere at 450 ˚C for 4.0 h (hydrogen flow rate: 100 $mL\cdot min^{-1}$, heating rate: 2.0 $^{\circ}C\cdot min^{-1}$).

Dehydration catalyst: ThO_2 is directly calcined with $Th(NO_3)_4\cdot 6H_2O$ in a muffle furnace at 450 ˚C for 10 h.

Activity tests

Lipid hydrogenation to fatty alchols

Weigh 1.0 g oil, 0.2 g metal catalyst and 80 mL *n*-hexane into 300 mL Parr autoclave. Before inflating, first introduce the gas three times with N_2, and then three times with H_2. Flush into 5.0 MPa H_2, and react at 300 ˚C for 6.0 h at a stirring speed of 500 rpm. Liquid products were analyzed by Shimadzu QP-2010 Ultra's GC-MS, and the column model was Rtx-5Sil MS (30 m × 0.25 m × 0.25 μm). The method for GC detection follows, the initial temperature is set at 100 ˚C, with the heating rate of 10 ˚C/min to 280 ˚C, and maintained at this temperature for 42 min..

We used decalin as an internal standard to calculate the yields of products.

Conversion = (changes of reactant / total amount of reactant) × 100%.

Selectivity = (C atoms in each product / total C atoms in the products) × 100%.

Yield = Conversion × Selectivity × 100%.

Alcohol dehydration to α-olefins

Weigh 3.0 g fatty alcohol, add a certain amount of dehydration catalyst and 80 mL of *n*-hexane to a 300 mL Parr kettle. Before inflating, wash with N_2 three times, and react at 300 ˚C for 6.0 h at a stirring speed of 500 rpm.

Polymerization and hydrogenation of α-olefins to bio-lubricant base oil

1) Polymerization test: Put a certain mass of the prepared olefin in a water-treated

round-bottomed flask with nitrogen as protective gas, and then 5 % polymerization catalyst $AlCl_3$ was added. The reaction was heated to the required temperature, and lasting for 4.0 h. When the polymerization reaction was finished, we used the distilled water to quench the reaction. We washed the oil layer until pH was changed into neutral, and then the organic samples were separated and collected.

2) Hydrogenation test: Weigh 10.0 g bio-lubricant base oil precursor, 0.2 g Pd/C catalyst and 80 mL of *n*-hexane into a 300 mL Parr autoclave. Before inflating, first wash the gas three times with N_2, then three times with H_2, and then introduce 4.0 MPa H_2 at 250 ˚C at a stirring speed of 500 rpm for 3.0 h. After distillation, the bio-lubricant base oil is obtained.

Catalyst characterization

The specific surface area and pore size distribution were performed by N_2 adsorption at 77 K on a Quantachrome Autosorb-3B instrument after activating the samples under vacuum at 573 K for 10 h.

Powder X-ray diffraction (XRD) patterns were measured on Rigaku Ultima IV X-ray diffractometer utilizing Cu K_α radiation ($\lambda = 1.5405$ Å) operated at 35 kV and 25 mA.

Transmission electron microscopy (TEM) images were performed on a FEI Tecnai G_2F_{30} microscope working at 300 kV.

The calcined samples were characterized by temperature-programmed reduction using a TP-5080 adsorption instrument (equipped with a TCD detector). The gas product was a mixed gas of 5 % H_2/He, and the heating rate was 5 ˚C $\cdot$min^{-1}.

Determination of properties of lubricants

The IR spectra were conducted on a Nicolet Nexus 670 FT-IR spectrometer in absorbance mode at a spectral resolution of 2 cm^{-1}. The IR spectra of the adsorbed CO (IR–CO) were recorded with a Nicolet NEXUS 670 FTIR spectrometer equipped with an in situ IR cell. The samples were reduced in H_2 at 623 K for 1 h, and then CO was adsorbed at room temperature.

^{1}H (400 MHz), NMR spectra were recorded on a Bruker AM-400 spectrometer using tetramethylsilane as an internal standard in $CDCl_3$.

The viscosity of the synthesized lubricants was determined according to the GB/T 265-88 standard, using the PND401A kinematic viscosity tester produced by Jilin

Prime Technology Co., Ltd. Viscosity index (VI) is a conventional value that represents the characteristics of the viscosity of petroleum products with time. The viscosity index is calculated according to "GB/T 1995-1998 Petroleum Product Viscosity Index Calculation Method".

Solidification point and pour point measurement: According to GB/T 510-2018 and GB/T 3535-2006, the solidification point and pour point of the synthesized lubricants were tested by using the PND176 petroleum product freezing point tester produced by Jilin Prime Technology Co., which was equipped with cold tank and glass test tube meeting the requirements.

The thermal gravimetric analyzer (TGA) and differential scanning calorimeter (DSC) test of bio-lubricant base oil was measured by METTLER TOLEDO, Approximately 5 mg of the sample rose from 35 ºC to 500 ºC at a temperature increase rate of 10 $^{\circ}\mathrm{C}\cdot\mathrm{min}^{-1}$ under the flow rate of 50 $\mathrm{mL}\cdot\mathrm{min}^{-1}$ air.

The friction coefficient and friction spot diameter were measured by MRS-1J Mechanical four-ball long-term anti-wear testing machine (Jinan Testing Machine Machinery Factory). Experimental conditions: room temperature, loading 392N, 1450 rpm/min, 30 min.

The contact angle test of bio-lubricant base oil was measured by Erma Contact Angle Meter, Japan.

Table and Figures Captions:

Fig. S1 Reaction path for selective conversion of lipid to fatty alcohols.

Fig. S2 a) N_2 adsorption–desorption isotherms of the prepared Ru-M/SiO_2 catalysts. b) Pore diameter distributions of the prepared supported Ru-M/SiO_2 catalysts.

Fig. S3 a) Hydrogen pressures Reaction conditions: 1.0 g palm oil, 0.2 g catalyst, 80 mL hexane, 300 ˚C, stirring at 500 rpm. b) Reaction temperature impact towards palm oil conversion and product distributions. Reaction conditions: 1.0 g palm oil, 0.2 g RuSn/SiO_2, 80 mL hexane, 5.0 MPa H_2, stirring at 500 rpm.

Fig. S4 Effect of substrate concentration on alcohol yield. Reaction conditions: 300 ˚C, 80 mL *n*-hexane, 5.0 MPa H_2, stirring at 500 rpm.

Fig. S5 a) XRD, b) H_2-TPR, c) CO-FTIR measurements on the prepared Ru-M/SiO_2 samples.

Fig. S6 HRTEM image of the prepared 1.5 wt.%Ru 6 wt.%Sn/SiO_2 catalyst.

Fig. S7 Mechanism of the hydrogenation of ester into alcohol over RuSn catalyst.

Fig. S8 Dehydration reaction over different catalysts. Reaction condition: 3.0 g *n*-octadecanol, 0.6 g catalyst, 80 mL hexane, 300 ˚C, 6.0 h, stirring at 500 rpm.

Fig. S9 The influence of calcination temperature on *n*-octadecanol dehydration. Reaction condition: 3.0 g *n*-octadecanol, 0.6 g nano-Al_2O_3, 80 mL hexane, 300 ˚C, 6.0 h, stirring at 500 rpm.

Fig. S10 TEM images of diverse Al_2O_3 samples.

Fig. S11 Recycling test of alcohol dehydration reaction over nano-Al_2O_3 and ThO_2 catalyst. Reaction condition: 3.0 g *n*-octadecanol, 0.6 g nano-Al_2O_3, 0.3 g ThO_2, 80 mL hexane, 300 ˚C, 6.0 h, stirring at 500 rpm.

Fig. S12 Polymerization mechanism of α-olefin over $AlCl_3$.

Fig. S13 a) TEM, b) N_2 adsorption–desorption isotherm, c) XRD, and d) pore diameter distribution of Pd/C catalyst.

Fig. S14 Flow diagram for the production of bio-lubricants from natural oils after tandem steps.

Scheme S1 Proposed reaction mechanism for intra-molecular stearic alcohol dehydration.

Table S1 Fatty acid composition of microalgae oil, palm oil, coconut oil, and soybean oil. Reaction conditions: 1.0 g oil, 1.0 g CaO, 100 mL methanol, 80 ˚C, 2.0 h.

Table S2 Textural properties of Al_2O_3 and ThO_2 catalysts.

Table S3 Comparative tribological experiments on commercial ExxonMobil 4T lubricant and prepared bio-lubricant from coconut oil.

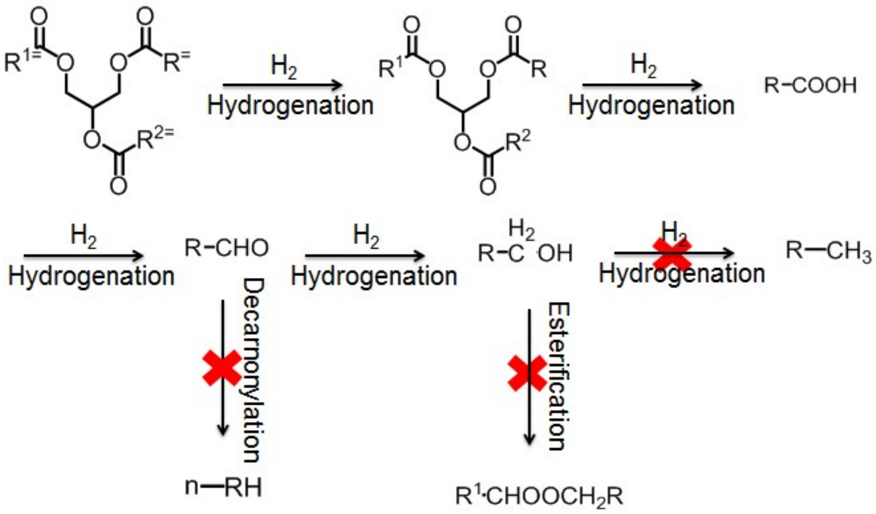

Fig. S1 Reaction paths for selective conversion of lipid to fatty alcohols.

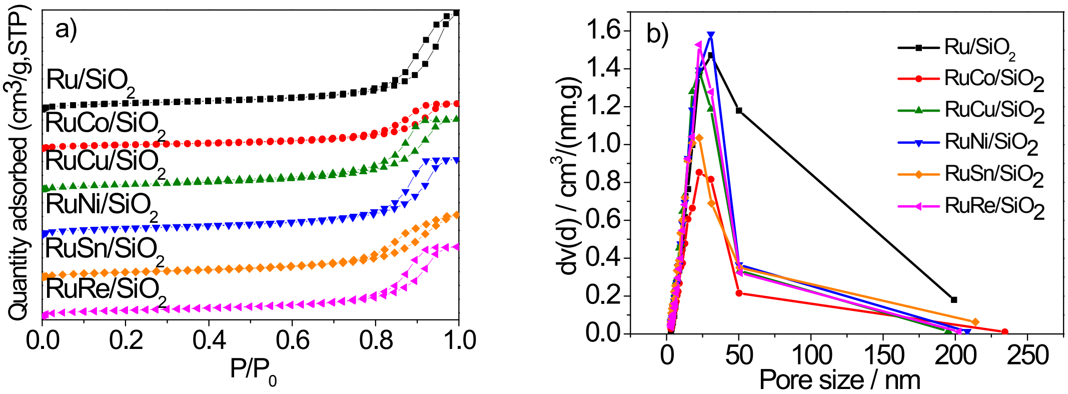

Fig. S2 a) N_2 adsorption–desorption isotherms and b) pore diameter distributions of the prepared Ru-M/SiO_2 catalysts.

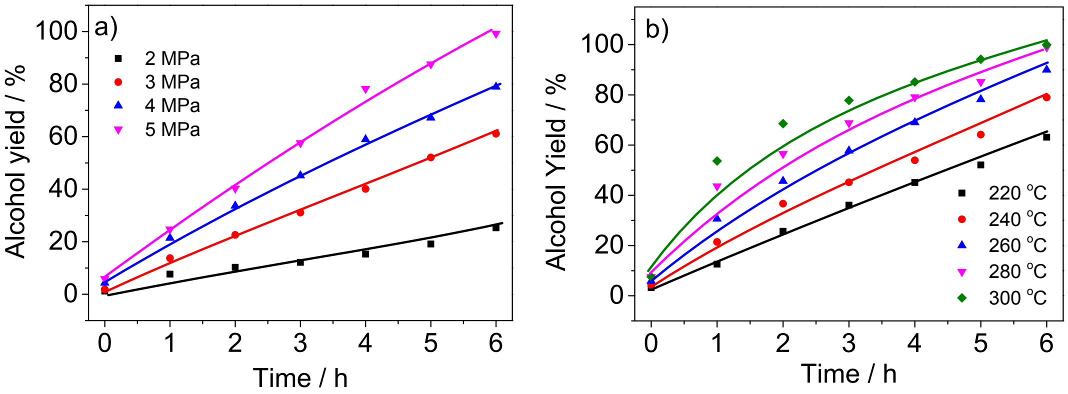

Fig. S3 a) Effect of hydrogen pressure on alcohol yield from palm oil hydrogenation. Reaction conditions: 1.0 g palm oil, 0.2 g catalyst, 80 mL *n*-hexane, 300 ˚C, stirring at 500 rpm. b) Reaction temperature impact on alcohol yield from palm oil hydrogenation. Reaction conditions: 1.0 g palm oil, 0.2 g RuSn/SiO_2, 80 mL *n*-hexane, 5.0 MPa H_2, stirring at 500 rpm.

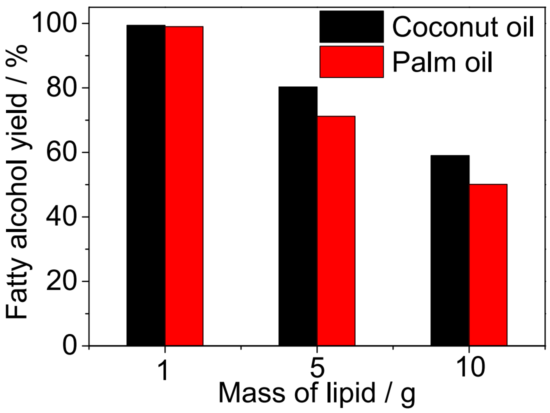

Fig. S4 Effect of substrate concentration on alcohol yield. Reaction conditions: 300 ˚C, 80 mL *n*-hexane, 5.0 MPa H_2, stirring at 500 rpm.

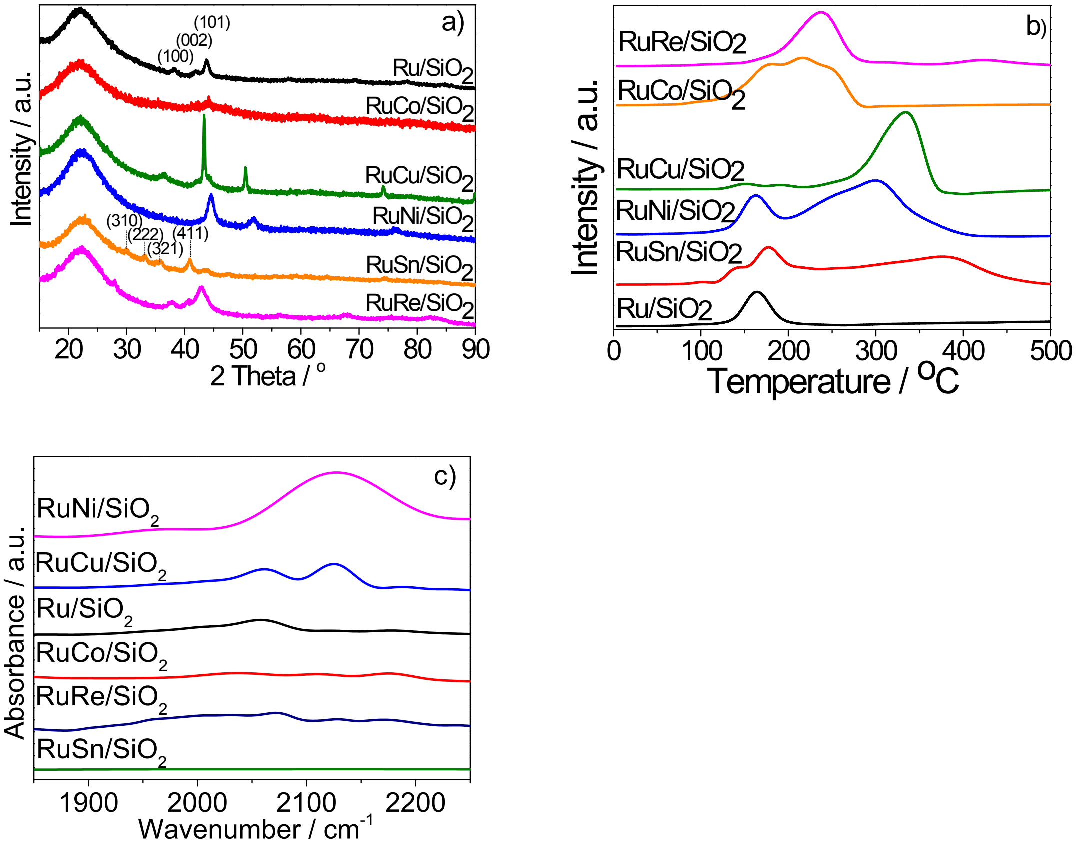

Fig. S5 a) XRD, b) H_2-TPR, c) CO-FTIR measurements on the prepared Ru-M/SiO_2 samples.

XRD patterns (Fig. S5a) showed the characteristic diffraction peaks of the Ru (100), Ru(002), Ru(101) and Ru(102) crystal facets. When the Sn element was added, the intensity of the characteristic diffraction peaks of Ru was decreased, and some new characteristic diffraction peaks appeared, corresponding to the Ru_3Sn_7 crystal planes of (310), (022), (321), and (411) (JCPDS # 26-0504).

H_2-TPR profiles (Fig. S5b) demonstrated that the single reduction peak of RuO appeared at ca. 150 ˚C on Ru/SiO_2. When the Sn element was added, the reduction peak of RuO became broadened, indicating that SnO_2 and RuO had certain interaction. In addition, a new reduction peak appeared at about 400 ˚C, suggesting a certain interaction with Ru and SnO_2. This partially reduced Sn enters the Ru atomic lattice to form Ru_3Sn_7 nanoclusters.

IR of adsorbed CO spectra (Fig. S5c) showed that a strong peak appeared at 2078 cm^{-1} for the single metal Ru/SiO_2 catalyst, and a broad peak appeared at 2016 cm^{-1}, respectively attributed to the infrared absorption peaks of $Ru^{\delta+}$-CO_2 and Ru^0-CO. When the Sn element is added, the absorption peak of CO disappeared, confirming the formation of Ru_3Sn_7 alloy, and Ru_3Sn_7 hindered the adsorption of CO by Ru.

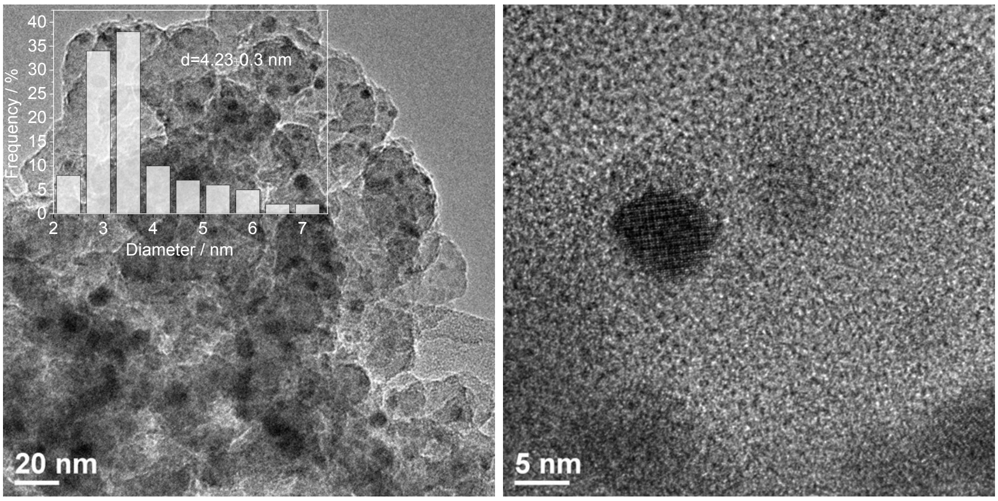

Fig. S6 HRTEM image of the prepared 1.5 wt.%Ru 6 wt.%Sn/SiO_2 catalyst.

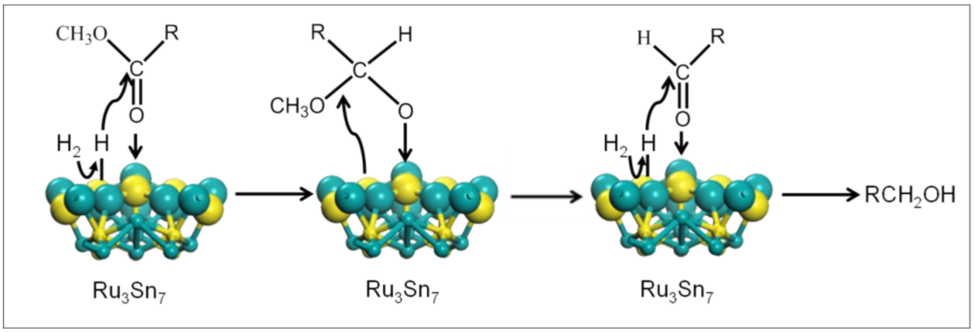

Fig. S7 Mechanism of the hydrogenation of ester into alcohol over RuSn catalyst.

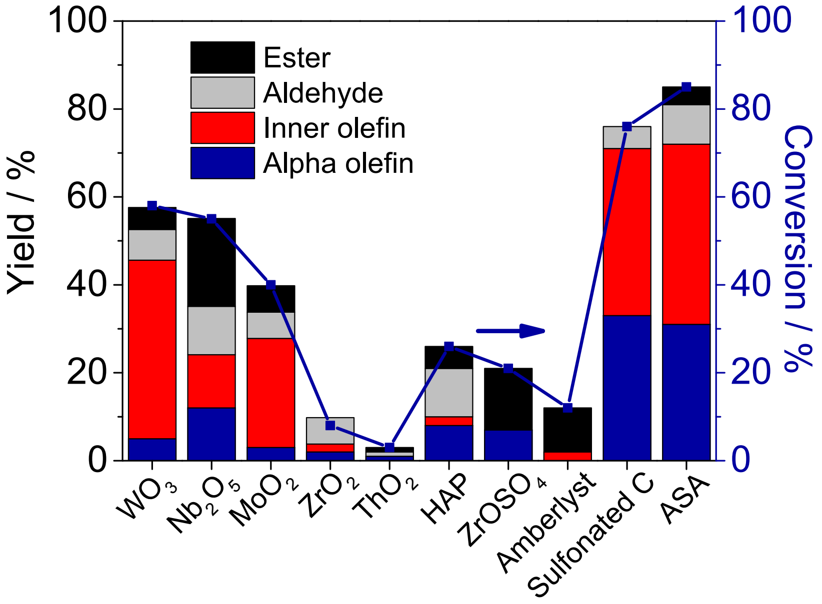

Fig. S8 Dehydration reaction over different catalysts. Reaction condition: 3.0 g *n*-octadecanol, 0.6 g catalyst, 80 mL hexane, 300 ˚C, 6.0 h, stirring at 500 rpm.

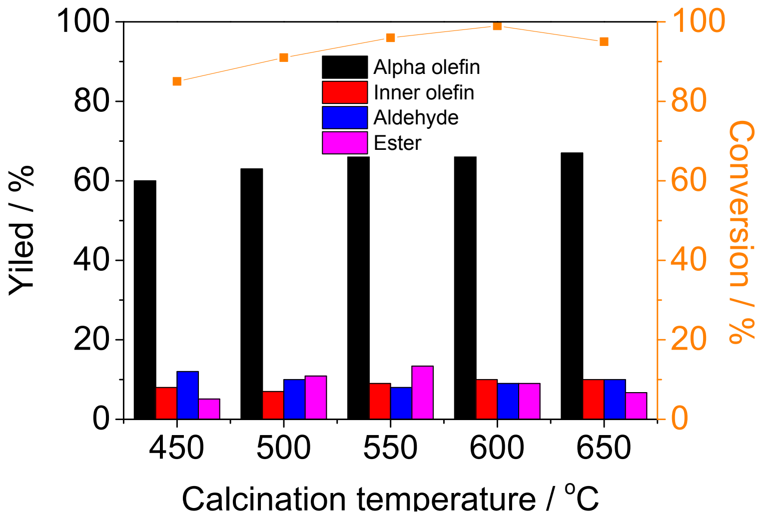

Fig. S9 The influence of calcination temperature on *n*-octadecanol dehydration. Reaction condition: 3.0 g *n*-octadecanol, 0.6 g nano-Al_2O_3, 80 mL hexane, 300 ˚C, 6.0 h, stirring at 500 rpm.

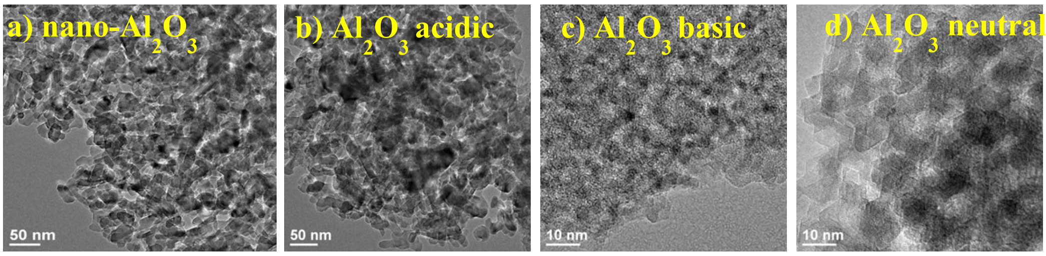

Fig. S10 TEM images of diverse Al_2O_3 samples.

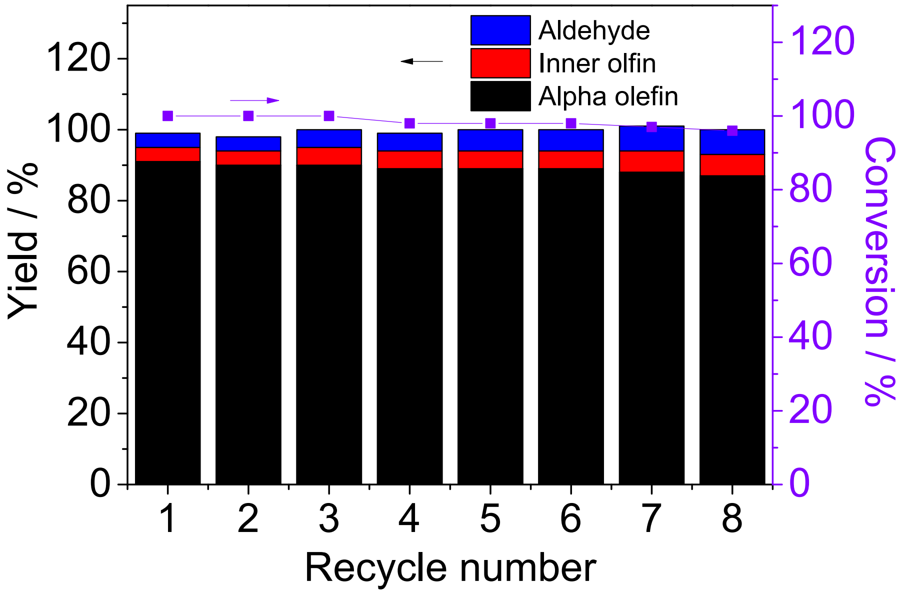

Fig. S11 Recycling test of alcohol dehydration reaction over nano-Al_2O_3 and ThO_2 catalyst. Reaction condition: 3.0 g *n*-octadecanol, 0.6 g nano-Al_2O_3, 0.3 g ThO_2, 80 mL hexane, 300 ˚C, 6.0 h, stirring at 500 rpm.

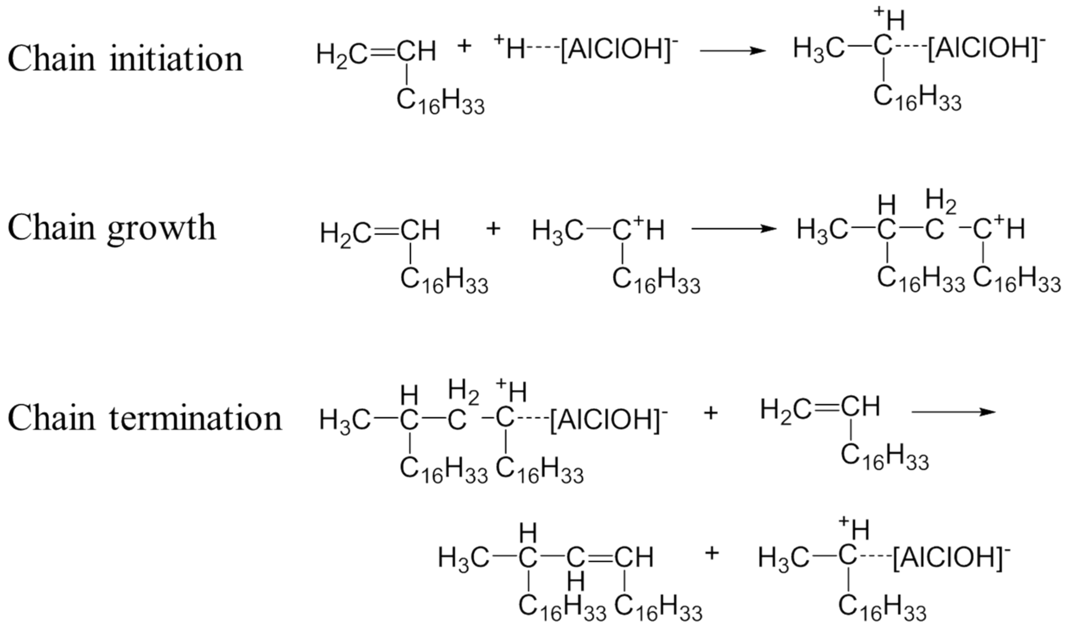

Fig. S12 Polymerization mechanism of α-olefin over $AlCl_3$.

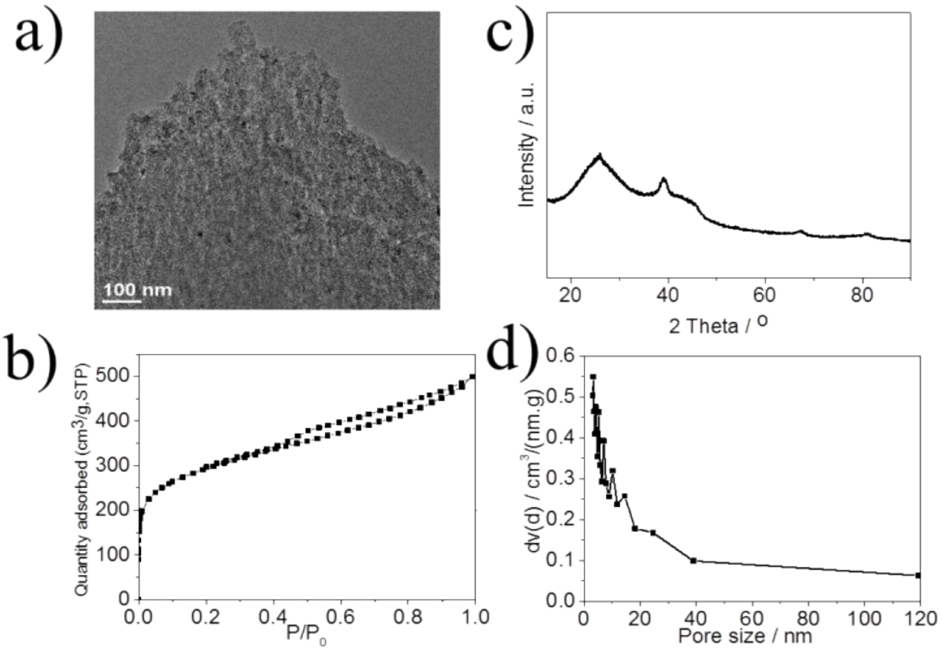

Fig. S13 a) TEM, b) N_2 adsorption–desorption isotherm, c) XRD, and d) pore diameter distribution of Pd/C catalyst.

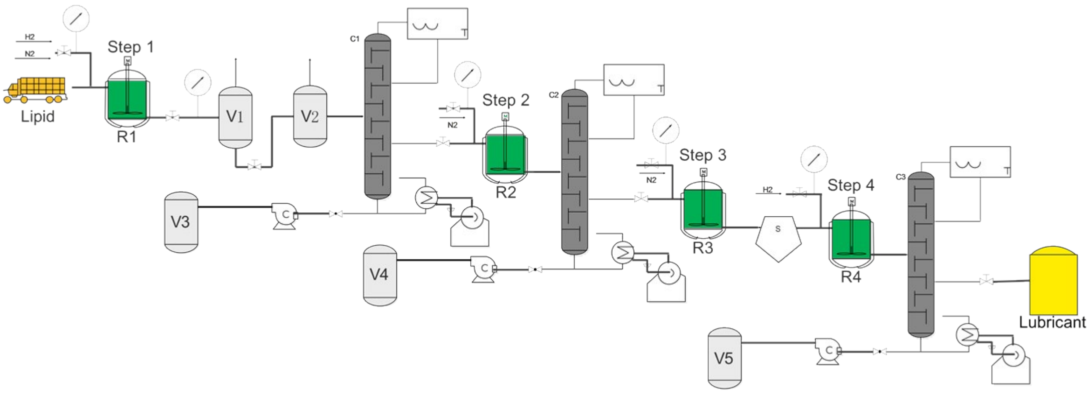

Fig. S14 Flow diagram for the production of bio-lubricants from natural oils after tandem steps.

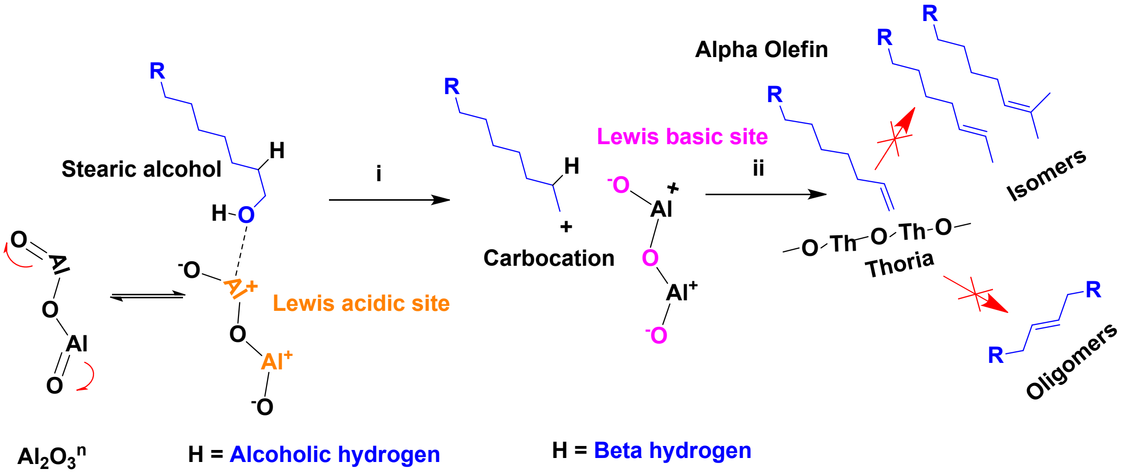

Scheme S1 Proposed reaction mechanism for intra-molecular stearic alcohol dehydration.

Table S1. Fatty acid composition of microalgae oil, palm oil, coconut oil, and soybean oil. Reaction conditions: 1.0 g oil, 1.0 g CaO, 100 mL methanol, 80 ˚C, 2.0 h.

① Fatty acid composition of microalgae oil

Type	$C_{6:0}$	$C_{8:0}$	$C_{10:0}$	$C_{12:0}$	$C_{14:0}$	$C_{16:0}$	$C_{18:0}$	$C_{18:1}$	$C_{18:2}$
Content / %	0.04	4.41	4.41	32.2	56.2	0.43	0.07	0.44	0.97

② Fatty acid composition of palm oil

Type	$C_{14:0}$	$C_{16:0}$	$C_{18:0}$	$C_{18:1}$	$C_{18:2}$	$C_{20:0}$	-	-	-
Content / %	1	40.7	5.7	48.4	3.8	0.2	-	-	-

③ Fatty acid composition of coconut oil

Type	$C_{6:0}$	$C_{8:0}$	$C_{10:0}$	$C_{12:0}$	$C_{14:0}$	$C_{16:0}$	$C_{18:0}$	$C_{18:1}$	$C_{18:2}$
Content / %	0.7	9.5	6.2	46	16.5	9.4	2.4	7.6	1.7

④ Fatty acid composition of soybean oil

Type	$C_{16:0}$	$C_{16:1}$	$C_{16:2}$	$C_{18:0}$	$C_{18:1}$	$C_{18:2}$	$C_{18:3}$	$C_{20:0}$	$C_{20:1}$
Content / %	7.8	0.1	0.1	3.0	36.6	48.8	2.5	0.4	0.5

Table S2. Textural properties of Al_2O_3 catalysts.

Catalyst	BET Surface area (m^2/g)	Pore volume (cm^3/g)	Pore size (nm)	Acid *conc.* By IR- Py (mmol/g)		Base *conc.* By CO_2-TPD (mmol/g)
				LAS[a]	BAS[b]	LBS[c]
Al_2O_3 acidic	197	0.26	4.2	0.14	0.0	0.13
Al_2O_3 basic	172	0.23	4.3	0.11	0.0	0.18
nano-Al_2O_3	361	0.47	38.0	0.46	0.0	0.57

[a]LAS: Lewis acid sites; [b]BAS: Brönsted acid sites; [c]LBS: Lewis base sites.

Table S3. Comparative tribological experiments on commercial ExxonMobil 4T lubricant and prepared bio-lubricant from coconut oil.

	bio-lubricant [a]	Exxon-Mobil 4T lubricant
Friction coefficient	0.078	0.098
Diameter of the friction spot (nm)	0.513	0.492

[a] prepared from coconut oil.